IEEE Access
Multidisciplinary | Rapid Review | Open Access Journal

SPECIAL SECTION ON GIGAPIXEL PANORAMIC VIDEO WITH VIRTUAL REALITY

Received July 8, 2020, accepted July 23, 2020, date of publication July 30, 2020, date of current version August 13, 2020.

Digital Object Identifier 10.1109/ACCESS.2020.3012997

Road Identification Algorithm for Remote Sensing Images Based on Wavelet Transform and Recursive Operator

CHEN GUOBIN[1], ZENGWU SUN[2], AND LI ZHANG[1]

[1]Chongqing Key Laboratory of Ecological Environment Spatial Information Data Mining and Big Data Integration, Rongzhi College, Chongqing Technology and Business University, Chongqing 401320, China

[2]College of Medical Information Engineering, Shandong First Medical University and Shandong Academy of Medical Sciences, Taian 271016, China

Corresponding author: Zengwu Sun (sunzengwu@aliyun.com)

This work was supported in part by the Chongqing Municipal Education Commission Science and Technology Project under Grant KJZD-K201902101 and Grant KJZD-K201802101, and in part by the Humanities and Social Sciences Project of Rongzhi College, Chongqing Technology and Business University under Grant 20197004.

ABSTRACT Road edge detection from remote sensing images, as an important ground object type, plays an important role in people's life and travel and urban planning and development, and extracting road information from remote sensing images has practical scientific value and practical significance. However, with the development of remote sensing technology, while the resolution of remote sensing images is improved, the information describing ground objects becomes more and more abundant, and the difficulty of identifying and extracting road information is also increased. In the process of acquiring remote sensing images, the actual system is subjected to various kinds of noise interference. Different environmental interference and system defects will introduce noises with completely different distribution and statistical characteristics to remote sensing images. Aiming at the problem that the detection effect of traditional algorithms becomes worse due to the influence of noise on remote sensing images, a wavelet transform denoising method and morphological gradient operator are proposed. By selecting appropriate structural elements of remote sensing images, noise pixels cannot participate in morphological calculation, and the noise intensity changes with the size of quantum superposition state structural elements. Therefore, a morphological gradient operator is established and applied to edge detection of remote sensing images. Finally, the experimental results show that the method proposed in this article is better than other directions in terms of effect through road edge detection and matching. This method can effectively reduce noise. Compared with other algorithms, the method proposed in this article has certain advantages.

INDEX TERMS Radar remote sensing image (RRSI), noise interference, gradient operator; edge detection control, outage probability.

I. INTRODUCTION

Remote sensing technology is a kind of detection technology that arose in the 1960s. Based on the characteristics of electromagnetic waves radiated by long-range targets, A variety of cutting-edge sensing instruments are used for acquisition, And the collected information is processed and imaged through certain technical conversion, Therefore, a technical means for analyzing, identifying and comprehensively applying various ground object information benefits from the rapid development of remote sensing technology [1]. The spatial resolution of remote sensing images is getting higher and higher, and the detailed information of ground objects is getting richer and richer. The accompanying noise interference is becoming more and more serious. These changes have limited the application of many traditional target object extraction methods to high-resolution remote sensing images. It is more difficult to extract target objects from high-resolution remote sensing images at all levels. This article is to carry out its own research work on the basis of this problem and explore new methods to adapt to the rapid development of remote sensing technology.

As an important feature type, it is one of the basic features with the fastest information update. Compared with the

The associate editor coordinating the review of this manuscript and approving it for publication was Zhihan Lv.

traditional road information collection methods, Road information detection method based on remote sensing image, the cost is lower; the wide coverage makes up for the disadvantages of traditional collection methods, the road information with good real-time and high accuracy can be obtained [2]. On this basis, through the acquisition of road information and the mining of later data, it plays an important role in urban regional planning, traffic information management, vehicle travel guidance and vehicle navigation positioning. Therefore, using high-resolution remote sensing data to extract road information quickly and accurately has very important theoretical significance and practical value in the long-term development of people's living environment and travel convenience, which is embodied in the following aspects:

(1) Urban and road network planning: Road survey and identification can provide a convenient and effective data basis for road network planning and management, and is the theoretical basis for decision-making on the rational operation and maintenance status of road network planning. At the same time, it also reflects the distribution of various infrastructures in the current developing city from the side and provides help for urban planning.

(2) Traffic Guidance Management: Road information can provide detailed and scientific data support for the management of various traffic problems. Through a series of technical means, It can obtain more comprehensive and accurate road information with good real-time performance, thus providing a data basis for the strict management and scientific management of traffic travel by government management departments and building a safe, smooth, harmonious, civilized and efficient traffic environment.

(3) Emergency protection for dangerous situations: It can improve the ability of government agencies to deal with emergencies, disasters and emergencies. In view of the frequent occurrence of various natural disasters caused by malignant changes in the natural environment, such as Honggang typhoon, ice disaster and earthquake, As well as the occurrence of man-made disasters such as war and terrorist attacks, remote sensing technology can quickly understand the real-time situation of road traffic in disaster areas, providing data information and decision support for emergency disposal, disaster mitigation and post-disaster reconstruction.

As an important source of road information, Real-time and accurate road information can be obtained through high-resolution remote sensing images. This information provide data support for information collection of Intelligent Transportation System (ITS) and subsequent database construction, help to improve the operation efficiency of transportation system, and play an important role in urban development, social stability and people's life.

Due to the complex scene of remote sensing images and the large amount of interference from ground objects, it is difficult to extract roads, at present, most of the existing road extraction schemes are based on various methods. The current research trend is that, In order to extract road information effectively and accurately in practical applications, it is necessary to base on the characteristics of different images. On the basis of analyzing the principles and applicable conditions of various road extraction methods, The methods are compared and improved, The general process of road extraction method can be summarized as follows: firstly, the road is roughly extracted to obtain the basic contour, and then the corresponding method is adopted to trim and refine to obtain a purer road area.

II. RELATED WORK

Due to the influence of factors such as instrument manufacturing and the surrounding environment [3], remote sensing images will inevitably contain noise. Therefore, it is often necessary to denoise RRSI when performing image processing. At present, the processing of remote sensing images mainly considers Gaussian noise [4] and impulse noise [5]. The image with noise affects the judgment of the staff, and the denoising technique extracts the original image to complete the image better interpretation. At present, the principle of wavelet transform plays a more important role in image denoising. The wavelet denoising method is simple to use and the image processing quality is better. Therefore, wavelet denoising has become a common denoising method. In the development of wavelet denoising technology, domestic and foreign scholars are constantly trying to develop new denoising algorithms. Wavelet and morphological edge detection have also been greatly developed and promoted in the application of image edge detection, scholars D. Kincaid and W. Cheney applied mathematical morphology to edge detection [6], thus form a system of edge detection for mathematical morphology. The method of joint detection is developed by scholars to overcome the limitations of a single method and avoid the defects of a single method. In 2014, J. Zhang proposed an edge detection algorithm based on wavelet NSCT transform and morphology [7].

Most techniques use Sobel, Roberts, Prewitt and other operators to approximate the first-order image gradient. It is difficult to obtain a good boundary for edge detection in noisy images because both noise and edge contain high frequency content [8]. Convolution operators used on noisy images usually have a large range because they can average enough data to eliminate local noisy pixels [9]. It can be seen that the image segmentation technology using edge detection is suitable for the situation where there are significant differences between the internal regions of the image. Therefore, the research focus of researchers at home and abroad in the past is mostly on the anti-noise performance and detection accuracy of balanced edge detection algorithms. If the anti-noise performance is overemphasized, the edge and contour of the image will have large errors and deviations. If the processing accuracy of edge detection is overemphasized, it may result from the image boundary where the original image does not match [10].

A part of the image always shows discontinuous gray or color values or at least large feature changes, which is

called the boundary (edge) between the object area (target and background). Such image features are an important means to obtain image edges. Edge detection [11] can highlight the target in the image from the background. The segmentation method based on edge detection mainly uses operators to extract edges containing different regions, thus realizing image segmentation [12]. Edge detection is generally divided into three steps: firstly, some edge detection operators are used to detect possible edge points in the image; Secondly, complex edge refinement is carried out on the edge with a certain width to obtain a boundary line with a pixel width. Finally, the edge closing technology is used to obtain the closed edge. Edge detection aims to classify and locate discontinuities in images. The appearance of noise leads to high frequency in its field, which makes edge detection based on image gradient produce errors. The main purpose of studying various edge detection technologies and analyzing their performance is to solve the problems of pseudo edge detection, image noise, edge loss, etc. The image segmentation algorithm based on image edge detection divides the original image into meaningful regions by constructing continuous closed boundaries. This technology effectively reduces the amount of processing computation and also protects the structural information inside the region.

Super pixel aims to solve this problem by representing images in a more reasonable way, grouping pixels based on homogeneity criteria and restoring object boundaries. This provides a different representation of each image, where the boundaries are irregular and the super pixels have different sizes. This is achieved by over-segmentation of the image, which is a process of reducing the image into a plurality of regions by covering the image in such a way as to produce non-overlapping regions of uniform color [13]. Superpixels can be defined as spatially coherent uniform structures. Classic super-pixel segmentation methods include watershed algorithm, which has been proved to be a very useful and powerful tool in many different application fields, especially in remote sensing image segmentation. The watershed-based image segmentation algorithm uses the concept of topology, regards the gradient of the image as the terrain surface, and represents the pixels with higher gradient as continuous boundaries. The gray level of the image represents the height of the terrain, and the local minimum value of the gray level constitutes the low-lying basin in the terrain. Water collects inside each basin. When water reaches the boundary of the basin, the adjacent basins will merge together. By establishing dams at the boundary, the separation and isolation between adjacent basins are maintained. These connected and independent catchments are sub-regions after image segmentation.

In practice, watershed is often applied to image gradient [14], and watershed lines are used to separate uniform regions, thus giving the expected segmentation results [15]. Morphological gradients are usually used to obtain transformed gradient images. However, noise in gradient images often leads to over-segmentation, which will have a significant adverse impact on the quality of segmentation results [16]. The quality of gradient extraction directly affects the segmentation performance of this technology. With the help of peak signal-to-noise ratio, the results of watershed algorithm under different gradients are obtained. Therefore, using the standard morphological watershed transform [17] on the original image or its gradient, we usually obtain the result of over-segmentation. In order to reduce the excessive segmentation of watershed technology, several methods have been proposed in relevant foreign literatures. We can refer to labeling-based technology, region merging method [18], scale space method [19], image denoising or edge enhancement based on partial differential equation [20], wavelet technology combined with watershed transform [21], etc. In addition, other scholars have also put forward some suggestions to improve the over-segmented watershed, using space constraint technology to apply to the watershed (SCOW) [22]. The algorithm uses the concept of space to constrain, and then adopts the method of uniform labeling to realize compact and uniform distribution of super pixels, while significantly improving the processing speed. Although there are many different watershed algorithm solutions, there are still many problems to be solved. Therefore, the relevant research literature has been increasing in the past few years. In other words, watershed algorithm is still an open problem, and more and more new fields begin to use and develop this technology from different angles.

With the wide application of RRSI, edge detection has become particularly important in RRSI processing, especially in feature detection and feature extraction [23]–[25]. This is because the edge of the image carries most of the information of the image and can reflect the structural information of the image. The goal of RRSI edge detection is to find the discontinuity of RRSI mapping, and thus detect the edge position of different texture regions of RRSI [26]. The earliest RRSI edge detection methods used gradient class algorithms such as Sobel [27], prewitt [28], Canny [29], Laplacian of Gaussian [30]. These algorithms are for edge detection of optical images method. Since the edge detection method of optical image is processed for additive noise, the noise RRSI model is multiplicative noise, which makes the classical gradient edge detection method directly used for edge detection of RRSI difficult to achieve ideal results. False alarm rate is an important factor to measure the edge detection performance of RRSI. The classical gradient method is not a Constant False Alarm Rate (CFAR) for RRSI. Therefore, the research on edge detection of RRSI is imminent, and it is verified that the algorithm has good edge detection and localization ability.

Aiming at the above problems, this article proposes a wavelet denoising and a new morphological gradient operator. Compare by experiment has strong anti-noise ability under certain conditions, and can detect the edge of the contaminated image even when the noise intensity is large. The structure of the paper is as follows: The first part introduces the related research work; the second part introduces the

noise removal processing of the related images; the third part explains the morphological gradient operator; the fourth part compares the method proposed in this article with other methods.

III. RADAR REMOTE SENSING IMAGE FRACTAL WAVELET DENOISING MODEL

A. FBM MODEL

Fractal Brownian motion and fractal Gaussian noise is a mathematical model of statistical self-similar process proposed by Hewu in, which is an extension of Brownian motion process. At first, it was mainly used to describe the irregular shapes of mountains, clouds, topography and simulating the surface of planets in nature. Now it has been widely used in many fields such as image processing, information security, virtual reality and economy. In the aspect of network traffic modeling, the model only needs three parameters of coefficient, traffic average arrival rate and traffic variance coefficient to describe a long correlation sequence. It is the simplest and easiest to solve self-similar network traffic model. It plays a very important role in the theoretical research of network traffic self-similarity. From the definition of Brownian motion, we know that Brownian motion can be generated by the accumulation of Gaussian random variables, and the generation algorithm of Brownian motion is also proposed based on this idea. Because Brownian motion has the important property of statistical self-similarity, the random midpoint displacement algorithm (MPD) is produced to describe Brownian motion approximately. The algorithm is easy to implement and has good effect, so it has been widely used. The derivation process of generating one-dimensional Brownian motion curve by MPD algorithm is as follows.

On the interval [0, 1], if X(0) = 0, X(1) is a random variable sample with a mean value of 0 and a variance of σ^2, and then the variance of its increment is defined as:

$$Var(X(1) - X(0)) = Var(X(1)) = \sigma^2, \tag{1}$$

At this time, according to the characteristics of self-similarity, for any $0 \le t_1 \le t_2 \le 1$, there must be a formula

$$Var(X(t_1) - X(t_2)) = |t_1 - t_2| = \sigma^2, \tag{2}$$

If $X(\frac{1}{2})$ is the sum of the average values of $X(0)$ and $X(1)$ a Gaussian random disturbance D_1, and the average value of D_1 is 0 and the variance is Δ_1^2, that is:

$$\begin{cases} X(\frac{1}{2}) = \frac{1}{2}(X(0) + X(1)) + D_1 \\ E(D_1) = 0 \; and \; Var(D_1) = \Delta_1^2, \end{cases} \tag{3}$$

Substituting formula (2) to formula (1) has:

$$\begin{aligned} Var(X\left(\frac{1}{2}\right) - X(0)) &= Var\left[\frac{1}{2}(X(0)+X(1)) + D_1 - X(0)\right] \\ &= \frac{1}{4}\sigma^2 + Var(D_1) = |\frac{1}{2} - 0| = \sigma^2, \end{aligned} \tag{4}$$

Solvable: $Var(D_1) = \frac{1}{4}\sigma^2$ can be considered to be also applicable to interval [1/2, 1].

Further, let $X(\frac{1}{4}) = \frac{1}{2}\left[X(0) + X(\frac{1}{2})\right] + D_2$ and $E(D_2) = 0$.

By the same token, $Var(D_2) = \frac{1}{8}\sigma^2$ can also be considered applicable to other intervals. By analogy, there are the following rules:

$$\Delta_n^2 = \frac{1}{2^{n+1}}\sigma^2. \tag{5}$$

In Equation (5), Δ_n^2 is the variance of the midpoint offset. Therefore, corresponding to the independent variable $t_n = 2^{-n}$ of the interval [0, 1], a Brownian motion curve can be generated on the interval [0, 1] by adding a random disturbance with an expected value of 0 and a difference of Δ_n^2 to the corresponding random variable $X(t_n)$.

There are m regional block similarities in the RRSI, where node O is the central convergence, node an is the data source, and the service flow is sent from node an to node O, and then forwarded through node O. Traditional methods for characterizing business flow performance include Poisson model and Gaussian distribution. Based on the Fractal Brown Motion (FBM) model, the following model is proposed:

$$\begin{aligned} B^H(t) = \frac{1}{\Gamma(H+0.5)}\{&\int_{-\infty}^{0}[(t-\tau)^{H-0.5} - (-\tau)^{H-0.5}]dB(t) \\ &+ \int_0^t (t-\tau)^{H-0.5}dB(t)\}, \end{aligned} \tag{6}$$

$$\nabla B^H(t) = B^H(t) - B^H(t-1) = \int_{-\infty}^{1} K_H(t-u)dB(u), \tag{7}$$

where m is the average arrival rate, $\Gamma(*)$ is the γ function, H is the correlation parameter ($0 < H < 1$), B is the standard fractal Brownian motion, BH is the discrete fractal Gaussian noise model, and the function KH is:

$$K_H(u) = \begin{cases} u^{H-0.5} & 0 < u < 1 \\ u^{H-0.5} - (u-1)^{H-0.5} & u > 1. \end{cases} \tag{8}$$

From equation (1), $B^H(at) = a^H B^H(t)$ all mean values are 0, the variance is $\sigma^2 t^{2H}$, and the autocorrelation function is shown in equation (4).

$$r(t) = \sigma^2(t^{2H} + s^{2H} - |s-t|^{2H})/2, \tag{9}$$

The probability density function of FBM is:

$$f_{B_H}(x,t) = -\frac{1}{\sqrt{2\pi t^{2H}}}e^{(-\frac{x^2}{2t^{2H}})}, \tag{10}$$

where $\nabla B^H(t)$ in Equation 2, obeying the Gaussian distribution of $N(0, \sigma^2|\tau|^2)$, where σ^2 sees Equation 6:

$$\sigma^2 = E\{|B^H(1)|^2\} = \Gamma(1-2H)\cos(\pi H)/\pi H. \tag{11}$$

1.2 Wavelet Threshold Denoising

Generally speaking, the signals taken directly have certain noise. In most cases, we think that this noise is Gauss white noise. Because the wavelet transform characteristics of signals and white noise are different, the method of eliminating

noise is wavelet denoising by using the variance and amplification of signals and white noise to be different with the characteristics of wavelet scale transform. With the increase of wavelet transform scale, the variance and increase of white noise will decrease, but the variance and increase of signal will not change. Donoho has done a lot of wavelet denoising experiments and proposed a threshold denoising method. Later generations then chose reasonable parameters to better solve the corresponding denoising problems in practical projects.

Deformation monitoring data is a signal including noise, and its mathematical model can be expressed as:

$$s(x) = f(x) + e(i), \quad i = 1, 2, \ldots, n, \tag{12}$$

In which, $s(x)$ represents deformation monitoring data, which includes real deformation and deterministic noise (such as system error), $f(x)$ represents real deformation and $e(i)$ is random noise. The reduction of $e(i)$ noise part in the signal is to denoise the signal or data S so that the real deformed signal $s(x)$ is separated from the signal $f(x)$. In deformation analysis, in order to make the monitoring data more truly reflect the internal change law; we often need to deal with noise. Generally speaking, noise signals are usually high-frequency signals, so real signals are those with relatively stable low-frequency signals. The denoising process of wavelet threshold method is shown in Figure 1. It can be divided into the following three steps:

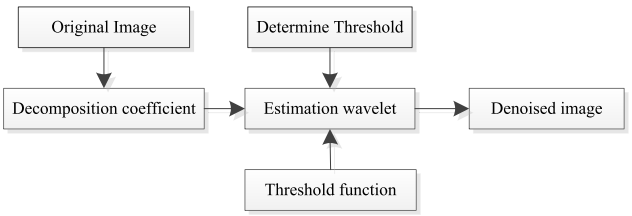

FIGURE 1. Wavelet threshold denoising flow chart.

(1) Wavelet decomposition. According to the actual engineering situation and the monitoring data collection situation, a reasonable wavelet basis function is selected, and then an appropriate decomposition layer N is selected to decompose the observation data in N layers.

(2) Threshold quantization. The threshold quantization processing here refers to the threshold quantization processing of wavelet decomposition high-frequency coefficients. There are many threshold selection rules. Its main purpose is to extract some effective signals from high-frequency signals, which can prevent useful signals from being mistaken for noise elimination in denoising.

(3) Wavelet reconstruction. According to the low-frequency coefficient of the N-th layer and the modified high-frequency coefficient from the first layer to the N-th layer, the denoised real data approximation can be obtained through signal reconstruction. In order to further improve the estimation accuracy, we generally reconstruct the Wavelet decomposition high frequency coefficients quantized by the threshold.

From the above steps, it can be seen that the selection method of the threshold and the quantization of the threshold can largely determine whether the image denoising quality is good or bad. The main basis of wavelet threshold denoising is that after wavelet transform, the data loses its original correlation, which will separate the signal from the noise. In the wavelet domain, the large coefficients are mainly signals, and the noise is scattered all over the whole.

Wavelet domain. Therefore, after wavelet transform processing, we can think that the wavelet coefficients with relatively large amplitude are signals, and the coefficients with relatively small amplitude are the noise we need to remove, so we can reduce the noise figure through threshold method and retain the signal coefficients we need.

Thresholds are divided into two categories, one is hard threshold and the other is soft threshold. Comparing the absolute value of the signal with the threshold, keeping the points greater than the threshold unchanged and setting the rest to zero, then we call it a hard threshold. Its expression is shown in Equation 13:

$$\omega_\lambda = \begin{cases} \omega, & |\omega| \geq \lambda \\ 0, & |\omega| < \lambda, \end{cases} \tag{13}$$

where λ represents the threshold, ω represents the size of the wavelet coefficients, and ω_λ represents the size of the wavelet coefficients after the threshold is given. The soft threshold is somewhat different from the hard threshold, and its expression is shown in Equation 14:

$$\omega_\lambda = \begin{cases} sign(\omega)(|\omega| - \lambda, & |\omega| \geq \lambda \\ 0, & |\omega| < \lambda, \end{cases} \tag{14}$$

When the absolute value of the wavelet coefficient is less than the threshold, the wavelet coefficient is set to zero. The difference is that when the absolute value of the wavelet coefficient is greater than or equal to the threshold value, the wavelet coefficient becomes the difference between the point and the threshold value. Such thresholds are called soft thresholds. Soft threshold is to subtract the threshold for wavelet coefficients greater than the threshold, instead of adopting a simple zero setting method for hard threshold, so that after soft threshold processing, the input and output curves are continuous. Therefore, in general, the signal curve processed by soft threshold is smooth, while the signal processed by hard threshold is rough, and the denoising effect of soft threshold is better than that of hard threshold.

The signal denoised by threshold method has two main characteristics: first, it better retains the characteristic spike points of the original signal; Second, the noise is almost completely suppressed. Wavelet transform can concentrate the signal on several wave coefficients, but white noise is still white noise no matter what orthogonal basis the transform is. Therefore, the wavelet transform coefficient value of the signal will definitely be larger than the wavelet transform

coefficient value of the noise, and then the signal will appear very prominent. If we can select an appropriate threshold to denoise the signal containing noise by threshold method, then we can achieve the purpose of denoising without distortion.

Adaptive Selection Threshold Based on Stein Unbiased Likelihood Estimation Principle. Firstly, the threshold likelihood estimation value is obtained, then the likelihood estimation value is minimized, and finally the selected threshold value is obtained. The specific steps are as follows:

Step1: Each element in the image takes an absolute value, sorts it from small to large, and then squares each element to generate a new sequence:

$$f(k) = sort(|s|)^2 \quad k = 0, 1, 2, \ldots, N-1, \tag{15}$$

where *sort* represents sort.

Step2: If the threshold is the square root of the k-th element of $f(k)$, there are:

$$\lambda_k = \sqrt{f(k)} \quad k = 0, 1, 2, \ldots, N-1, \tag{16}$$

The risk from this threshold is:

$$Rish(k) = \frac{1}{N}\left[N - 2k + \sum_{i=1}^{k} f(j) + (N-k)f(N-k)\right], \tag{17}$$

Step 3: According to the risk curve $Rish(k)$, the minimum risk point is recorded as $k_{\min}$, and the unbiased risk estimation threshold is defined as:

$$\lambda_k = \sqrt{f(k_{\min})}, \tag{18}$$

B. WAVELET NOISE PROCESSING OF RADAR REMOTE SENSING IMAGE

Let $\psi(\upsilon)$ denote a square integrable function ($\psi(\upsilon) \in L^2(R)$, wavelet mother function $\psi(\upsilon)$ satisfies:

$$\psi(\upsilon) = \int_T \frac{|\psi(\upsilon)|^2}{\upsilon} d\upsilon < \infty, \tag{19}$$

Wavelet $\psi(\upsilon)$ undergoes scale contraction and correlation scale function reconstruction to select appropriate wavelet function and scale function, see equation (8).

$$\begin{cases} \psi_{j,k}(t) = 2^{j/2}\psi(2^j t - k) \\ \delta_{j,k}(t) = 2^{j/2}\delta(2^j t - k), \end{cases} \tag{20}$$

The above equation becomes a pair of orthogonal bases, the signal $X(t)$, and see equation (21).

$$X(t) = \sum_K U_{j,k}\delta_{j,k}(t) + \sum_{j=j_0}^{\infty}\sum_k W_{j,k}\delta_{j,k}(t), \tag{21}$$

where the scale factor $U_{j,k}$ and the wavelet coefficient $W_{j,k}$, see equation (10).

$$\begin{cases} U_{j,k} = \int X(t)\delta_{j,k}(t)dt \\ W_{j,k} = \int X(t)\psi_{j,k}(t)dt, \end{cases} \tag{22}$$

where j represents the scale and K represents the different moving positions. The scale factor $U_{j,k}$ of the haar wavelet can be obtained by integrating the signal and the rectangular scale coefficient $\delta(t)$, and the signal is locally mean at $[k2^{-j}, (k+1)2^{-j}]$. $W_{j,k}$ indicates that the RRSI pixel has a local mean difference in the $[k2^{-j}, (k+1/2)2^{-j}]$ and $[(k+1/2)2^{-j}, (k+1)2^{-j}]$ regions, which varies from J to J+1, and the wavelet coefficient recursively sees equation (11):

$$\begin{cases} U_{j-1,k} = 2^{-1/2}(U_{j,2k} + U_{j,2k+1}) \\ W_{j-1,k} = 2^{-1/2}(U_{j,2k} - U_{j,2k+1}). \end{cases} \tag{23}$$

The inverse recursive transformation of Harr wavelet transforms the wavelet coefficients and scale coefficients at the coarse scale into fine scale coefficients and wavelet coefficients. The process is shown in equation (12).

$$\begin{cases} U_{j+1,2k} = 2^{-1/2}(U_{j,2k} + W_{j,2k}) \\ U_{j+1,2k+1} = 2^{-1/2}(U_{j,2k} - W_{j,2k}), \end{cases} \tag{24}$$

The above formula processes the discrete remote sensing image pixel $X(k)$ so that the pixel sequence length is 2^n, and the haar wavelet transform decomposes the finest scale coefficient $U_{n,k}$, and the relationship is shown in equation (25).

$$X(k) = 2^{-1/2}U_{n,k}, \quad k = 0, 1, \cdots, 2^n - 1. \tag{25}$$

The determination of the threshold has always been a research hotspot, which determines the degree of retention of information after image processing. The determination methods mainly include a given threshold denoising method, a global threshold method, and a Birge-Mas radar remote sensing t-policy threshold method. The given threshold denoising method is generally applicable to the source and type of noise, the occurrence period, etc. (these can be obtained by a large amount of statistical analysis). When more research is used, the threshold is calculated according to the empirical formula.

There are also some improvements in the threshold processing method. It can be seen from equations (13) and (14) that the hard threshold is processed in such a way that the wavelet coefficients are discontinuous near the threshold, and jump points are generated, and the soft processing method is obtained. The overall continuity of the wavelet coefficients is good, so that the estimated signal does not generate additional oscillation, but the high frequency information portion is lost, denoising process is as figure 2.

IV. MORPHOLOGICAL GRADIENT OPERATOR

A. A MORPHOLOGICAL GRADIENT OPERATOR

The method of mathematical morphology processing binary image is to regard binary image as a set, Binary images are detected by operations including intersection, union, complement and translation. When applying mathematical morphology to image analysis and processing, It is necessary to design a "probe" to collect image information. A "probe" is a set called structural element. It can be selected according to the purpose of image analysis, using structural elements

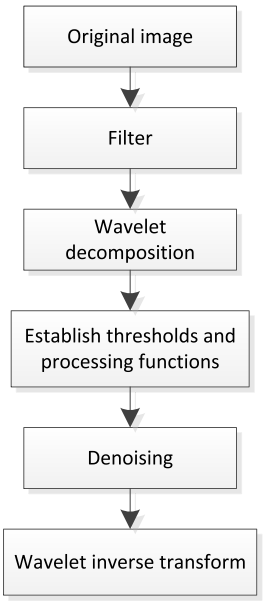

FIGURE 2. Wavelet denoising flow chart.

to transform various forms of image sets, to achieve the purpose of morphological analysis. Subsequently, In order to make the basic theory of morphology have more unified form and wider application, So as to facilitate the study of new algorithms, The core of the basic theorem of mathematical morphology is finally simplified to complete lattice structure. At the same time, Morphological methods applied only to sets have been extended to the field of numerical function analysis. The theory and method of gray morphology are produced. There are many methods to extend set operation to numerical function operation. Common methods include: The Umbra Approach and the Threshold Set Approach, and the complete lattice method to construct gray morphological operators as the minimum condition to satisfy the gray morphological operators. People have constructed a large number of operators by using gray morphology. It is widely used in gray image processing: in order to make morphology have better filtering properties, Sinha *et al.* introduced fuzzy mathematics into mathematical morphology to form fuzzy morphology; Then Wilson applied matrix morphology to character recognition, becoming an important direction of morphology. Morphology regards each pixel value of the color image as a vector when processing the color image, and uses the vector method to process each component with strong correlation to form the color image vector morphology.

The quantum state T in quantum mechanics can be described by vectors in the Hilbert space. Let 0 and 1 be two ground states, a multi-quantum system with n qubits and the i-th qubit state is equation (26):

$$\psi^i = \omega_0^i |0 + \omega_1^i |1 , \tag{26}$$

where ω_0 and ω_1 are the probability magnitudes of the ground states 0 and 1, respectively. The state ψ of the quantum is a tensor product of n qubit states, which can be expressed as equation (27):

$$\begin{aligned}\psi = \psi^1 \otimes \psi^2 \otimes, \ldots, \otimes \psi^n \ (\omega_o^1 \omega_0^2 \ldots \omega_0^n) |00 \ldots 0 \\ + (\omega_o^1 \omega_0^2 \ldots \omega_1^n) |00 \ldots 1 \ + \ldots + (\omega_1^1 \omega_1^2 \\ \ldots \omega_1^n) |11 \ldots 1 = \sum_{i=0}^{2^n - 1} \omega_i |i_b\end{aligned} \tag{27}$$

The symbol "$\otimes$" represents a direct product, i_b in the state vector $|i_b$ is an n-bit binary number corresponding to the decimal number i, and $|i_b$ represents the i-th ground state. ω_i is the probability magnitude of the ground state $|i$. For a multi-quantum system with n qubits, it is in basic state $|i >$ with different probabilities when it is not measured, but if it is evaluated, the state collapse and become 2^n ground states. One of the ground states.

Let $\omega_1^l = \sqrt{f_l}$, $\omega_0^l = \sqrt{1 - f_l}$, $\psi_l >= \omega_0^l |0 + \omega_1^l |1$ then the quantum superposition state structure be defined as:

$$B_q(x, y) = \begin{bmatrix} \psi^1 & . & \ldots & \ldots \\ . & . & \psi^l & \ldots \\ . & . & . & . \\ . & . & \psi^{n-1} & \psi^n \end{bmatrix}, \tag{28}$$

where $|\omega_1^l|^2 + |\omega_0^l|^2 = 1$, $|\omega_1^l|^2$ and $|\omega_0^l|^2$ respectively indicate the probability that ψ_l takes 1 and takes 0, that is, the probability that the structural element of the 1st point whose coordinate position is X is "1" and "0". Equation (28) can be expanded according to formula (19) as:

$$B_q(x, y) = \psi^1 \otimes \ldots \psi^l \ldots \otimes \psi^n. \tag{29}$$

In addition, there is at least one $\psi_1^l = 1, l \in \{1, 2, \cdots, n\}$ to ensure that the all-zero element is not contained in the quantum superposition state structure.

$M\ (x, y)$ is formed according to the local features of the image in the neighborhood of the pixel points (x, y) in the image, thereby representing the quantum measurement.

$$M(x, y) = |i_M(x, y) < i_M(x, y)| , \tag{30}$$

where $|i_M(x, y)$ represents a ground state collapsed after quantum measurement, and $|i_M(x, y) < i_M(x, y)|$ represents the outer product of the state vector $|i_M(x, y)$ and its transposed conjugate $< i_M(x, y)|$. If using $M\ (x, y)$ to measure (31):

$$\frac{M(x, y) |B_q}{\sqrt{< B_q |M^+(x, y) M(x, y) |B_q}} = \frac{\omega_i |i_M\ (x, y)}{\sqrt{\omega_i^2}} = |i_M\ (x, y), \tag{31}$$

where $M^+(x, y)$ in the above formula represents the transposed conjugate of $M\ (x, y)$, which collapses to the ground state $|i_M(x, y)$ after measurement, corresponding to the conventional structural elements. When the size and shape of the structural element window are determined, the morphological operation can be performed. $M\ (x, y)$ defined as follow.

Step 1: Normalize the image pixel values and set the structural element to 3×3;

Step 2: If the image pixel is a suspicious point (the pixel value is 0 or 1), set the structural element to 0, otherwise 1;

Step 3: If the structural element has only one point of 1, the expanded structural element window size is 5×5;

Step 4: If the structural element still has only one point of 1, continue to enlarge the window size of the structural element and increase it to 11×11.

For example, the image pixel value is $\begin{bmatrix} 0.5 & 0.5 & 0.6 & 0.5 \\ 0.3 & 1 & 0.5 & 0.8 \\ 0.2 & 0.3 & 0.4 & 0.8 \\ 0.2 & 0.2 & 0.4 & 0.3 \end{bmatrix}$; the coordinate origin of the structural element is the second row and the second column, and the pixel value is 1 to be a suspect point, and the quantum measurement operator $M(2,2) = |111101111 < 111101111|$ is set, and the measurement collapses to the ground state $|i_M(2,2) = |111101111$, and the quantum superposition state structural element For $\begin{bmatrix} 1 & 1 & 1 \\ 1 & 0 & 1 \\ 1 & 1 & 1 \end{bmatrix}$, let the structural element be B, and construct the morphological gradient operator according to the shape expansion operation and the morphological erosion operation, as equation (32).

$$\begin{cases} (f \oplus B)(x,y) \triangleq \max\{f(x-m, y-n), (m,n) \in B\} \\ (f \otimes B)(x,y) \triangleq \min\{f(x+m, y+n), (m,n) \in B\} \\ G(x,y) = (f \oplus B)(x,y) - (f \otimes B)(x,y), \end{cases} \tag{32}$$

The morphological gradient operator can be used for image edge detection. According to this, quantum collapse expansion operation and quantum collapse corrosion operation and quantum collapse morphological gradient operator for image edge detection can be constructed, as follows equation (33).

$$\begin{cases} (f \oplus B_q)(x,y) \triangleq \max\{f(x-m, y-n), (m,n) \in B_q\} \\ (f \otimes B_q)(x,y) \triangleq \min\{f(x+m, y+n), (m,n) \in B_q\} \\ G_q(x,y) = (f \oplus B_q)(x,y) - (f \otimes B_q)(x,y). \end{cases} \tag{33}$$

where B_q is a quantum superposition state structure.

The method in this article is to use binary morphological transformation to describe gray morphological transformation. First, the umbra of gray image or target signal and structural element is taken, their umbra is morphologically transformed, and then the surface is taken. The threshold method decomposes the gray image into a set of its threshold sets, which can be generated through a binary operation, and then these sets are used to synthesize and convert into a gray image.

B. GRADIENT BOUNDARY EXTRACTION

At present, people have proposed some edge detection operators based on mathematical morphology and applied them to image edge detection. The following introduces several commonly used morphological gradient operators, with F as the input gray image and G as the structural element. Several morphological gradients are defined as follows equation (34).

$$\begin{cases} Grad_1(F) = (F \oplus G) - F \\ Grad_2(F) = F - (F \odot G) \\ Grad_3(F) = (F \oplus G) - (F \odot G). \end{cases} \tag{34}$$

The above formulas are respectively called extended gradient operators, which subtract the original image from the expanded image to obtain the outer edge of the image. The non-extended gradient operator subtracts the etched image from the original image, and the obtained edge is the inner edge of the image. The extended gradient operator and the non-extended gradient operator are combined, and the difference between the two is obtained. It includes the outer edge and the inner edge of the image, so the edge is thicker.

Noise exists in any image. In the case of noise, The calculated difference along the i direction and the difference along the j direction can no longer fully reflect the gray level changes of actual ground objects. For remote sensing images, this problem is especially serious due to the existence of speckle. In order to reduce the influence of noise on boundary feature extraction, In remote sensing images and many other images, The grayscale changes at the boundary of objects with larger grayscale are also large, At the same time, the energy of noise in objects with large gray scale is also large. Therefore, using the average gray scale gradient to detect under the same threshold will produce serious missed detection in areas with low gray scale and serious false detection in areas with large gray scale. For this kind of image, using the relative average gray scale gradient to detect will have better effect.

V. EXPERIMENT AND ANALYSIS

A. EXPERIMENTAL COMPARISON

In the following, the most basic edge detection operator is used to detect image. Figure 2(a), 3(a), (https://pan.baidu.com/s/1MRLlFSBWQZc1la5bin6kxw, v5op), two remote sensing road images with different complexity levels are selected as examples and a variety of edge detection operators are compared. See Figures 3(b)-(e) and Figures 4(b)-(e). In the experiment, the same parameters were used in each step of the two example processes.

From the detection results in Figure 3 and Figure 4, it can be found that the edge continuity of the traditional Prewitt operator and the Sobel operator is poor, the data on the contour line is scattered, and the denoising ability is relatively poor, with more errors judging point. The edge effect extracted by the Sobel extension operator is improved compared with the traditional operator, but the definition and continuity of the contour are still not ideal. The edge details are not smooth enough, and there are still many burrs. The method has the best denoising effect, the detected contour is clear and the continuity is good, and the advantage in the curved section is obvious.

(a) The original image

(b) Denoising image

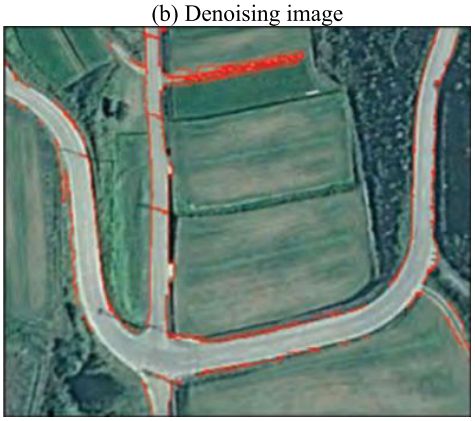

(c) Sobel operator

(d) Prewitt operator

FIGURE 3. Comparison of road edge retrieval effects of RRSI.

(e) Roberts operator

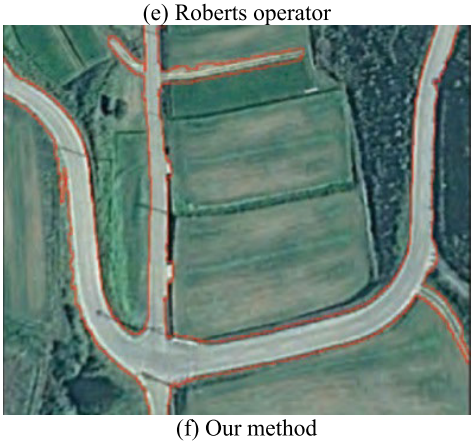

(f) Our method

FIGURE 3. *(Continued.)* Comparison of road edge retrieval effects of RRSI.

B. EXPERIMENTAL EVALUATION

Using MATLAB2016a for RRSI, using Sobel operators at different noise levels (0%, 10%, 20%, 30%, 40%, 50%, 60%, 70% and 80%), first 3×3 median filtering Roberts operator, Prewitt operator and wavelet and morphological gradient operator method proposed. Two evaluation criteria, objective criteria and subjective criteria were used to analyze the effects of various algorithms at different noise levels. In this article, the methods are judged by the normalized Mean Square Error (NMSE) objective evaluation index, which is defined as follows:

$$MSE = \frac{1}{M \times N} \sum_{i=0}^{M-1} \sum_{j=0}^{N-1} (x_{ij} - y_{ij})^2, \tag{35}$$

$$NMSE = \frac{MSE}{\sum_{x=0}^{M-1} \sum_{y=0}^{N-1} (y_{ij})^2}. \tag{36}$$

The height and width of the image are denoted by M and N respectively. x_{ij}, y_{ij} respectively, the noise image of the original image is denoised.

The ratio of signal value to noise value is a common evaluation method to measure denoising effect. Its unit is expressed in decibels. It is generally believed that the higher

(a) The original image

(b) Denoising image

(c) Sobel operator

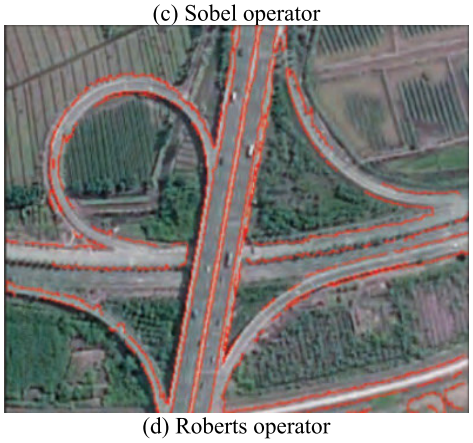

(d) Roberts operator

FIGURE 4. Comparison of edge retrieval results of RRSI overpass.

(e) Prewitt operator

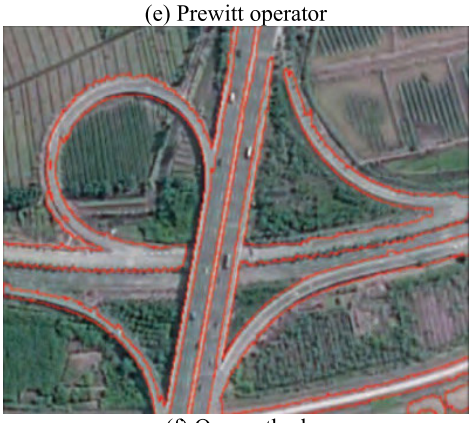

(f) Our method

FIGURE 4. *(Continued.)* Comparison of edge retrieval results of RRSI overpass.

the SNR, the better the denoising effect. It is defined as:

$$\begin{cases} P_s = \dfrac{1}{n}\sum_n f^2(n) \\ P_n = \dfrac{1}{n}\sum_{i=1}^{k}\left[f(i) - f'(i)\right]^2, \end{cases} \tag{37}$$

$$SNR = 10 \times \lg(\frac{P_s}{P_n}), \tag{38}$$

where P_s represents the power of the original signal; P_n is the noise power.

The signal-to-noise ratio gain refers to the ratio of the signal-to-noise ratio before and after wavelet denoising, and the expression is:

$$GSNR = {SNR_{dn}}/{SNR_n}, \tag{39}$$

SNR_{dn} represents the signal-to-noise ratio after denoising. SNR_n represents the signal-to-noise ratio before denoising. Like SNR, the larger GSNR, the better the denoising effect.

The normalized mean square error is calculated according to equation (36) as shown in Table 1. With the increase of impulse noise intensity, the Sobel operator increases the normalized mean square error and the worst anti-noise ability.

TABLE 1. Normalized mean square error (NMSE).

Noise intensity	Sobel intensity	Roberts intensity	Prewitt intensity	Our method
0%	0.0	6.5	24.2	0.0
10%	565.8	7.9	13.8	0.8
20%	671.6	15.1	13.8	1.4
30%	1234.4	43.3	19.8	3.2
40%	1567.3	126.3	43.1	5.6
50%	1674.9	278.3	78.2	9.3
60%	1765.4	445.1	123.8	17.9
70%	1875.9	723.4	163.3	15.6
80%	1898.8	1123.3	185.5	21.4

The Roberts operator is within 20% noise level, the normalized mean square error is small, and the edge detection capability is acceptable. The main error is due to the unfiltered noise, the 3 × 3 median filter changes significantly. Poor, normalized mean square error gradient; in the absence of noise, the first 3 × 3 median filter destroys the image details, and then the morphological gradient operator has a normalized mean square error of 6.5, and the edge detection reference image There is a certain deviation. The Prewitt operator has a normalized mean square error of at least 13.8 at 20% noise level, consistent with figures 3-4, and subjective evaluation criteria. Our method is consistent with the reference image result when the edge of the noise-free image is detected, and the normalized mean square error is zero. As the intensity of the impulse noise increases, the normalized mean square error increases slowly, consistent with the subjective evaluation criteria. Even when the impulse noise intensity is 80%, it can be detected. Compared with the edge of the noiseless image detected by the traditional morphological gradient operator, the normalized mean square error is 21.4.

Three technical indicators for measuring the performance of the algorithm are Spearman Rank Order Correlation Coefficient (SROCC), Pearson Linear Correlation Coefficient (PLCC) and Root Mean Square Error (RMSE), respectively. These measurements are used to measure the consistency of the method and other evaluation methods with subjective evaluation values. Because of the different range of quality evaluation values obtained by these methods, it is necessary to use the Logistic function for nonlinear fitting based on the scatter plot of the evaluation results.

Let the image size of the original image x and the distorted image y to be measured be. The SSIM algorithm defines the similarity between the brightness information, the contrast information, and the structure information between the two images as follows:

$$SSIM(x, y) = \frac{(2u_x u_y + c_1)(2\sigma_{xy} + c_2)}{(u_x^2 + u_y^2 + c_1)(\sigma_x^2 + \sigma_y^2 + c_2)}, \quad (40)$$

$$PSNR = 10\lg\left(\frac{MN*255^2}{MSE}\right), \quad (41)$$

where $u_x = \frac{1}{n}\sum_{i=1}^{n} x_i$ and $u_y = \frac{1}{n}\sum_{i=1}^{n} y_i$, σ_y are the variances of x and y, respectively, σ_x senting contrast information of image; σ_{xy} is the correlation coefficient of x and y, which characterizes the similarity of the structural information of the two images, c_1, c_2, c_3 is a small positive number, in case the denominator is zero.

Selecting three reference indicators PLCC, ROCC and SSIM is a good method for evaluation. From Table 2, the comparison of related performance is given. The method proposed in this article has the best effect on PLCC and ROCC, and the value on RMSE is the smallest. It can be seen that the prediction effect is close to the natural evaluation.

TABLE 2. Comparison with subjective assessment results.

Method	PLCC	RMSE	ROCC
SSIM	0.8654	0.5875	0.8876
PSNR	0.8213	0.6759	0.7342
GSNR	0.7765	0.5276	0.7532
Our method	0.9543	0.5432	0.8765

The overall evaluation method is obtained by comprehensively considering the first three indexes and adding them to the period of [0, 1]. Its expression is

$$HM = P_V M + P_{SNR} M + P_r M. \quad (42)$$

In this which, $P_V M$, $P_{SNR} M$ and $P_r M$ represent the normalized values of root mean square error, signal-to-noise

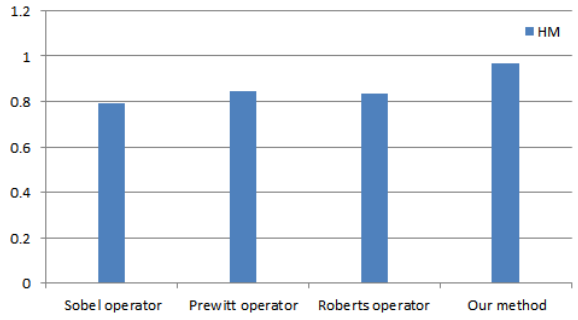

FIGURE 5. Comparison of Road HM with Four Algorithms.

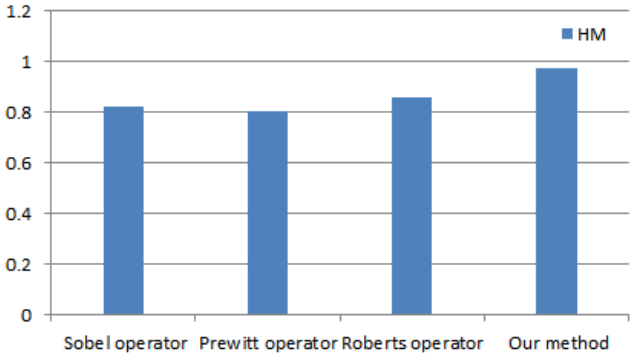

FIGURE 6. Comparison of Highway HM with Four Algorithms.

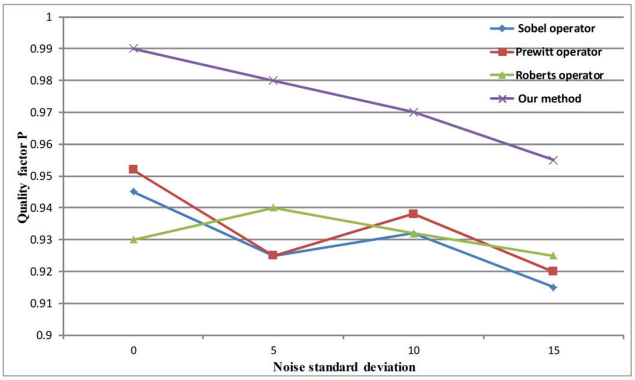

FIGURE 7. Comparison of road quality factor value and standard deviation.

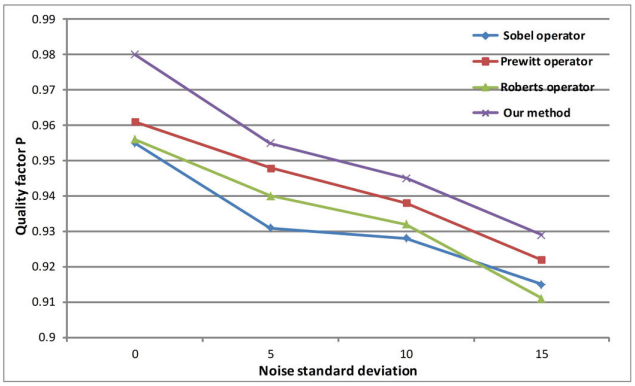

FIGURE 8. Comparison of highway quality factor value and standard deviation.

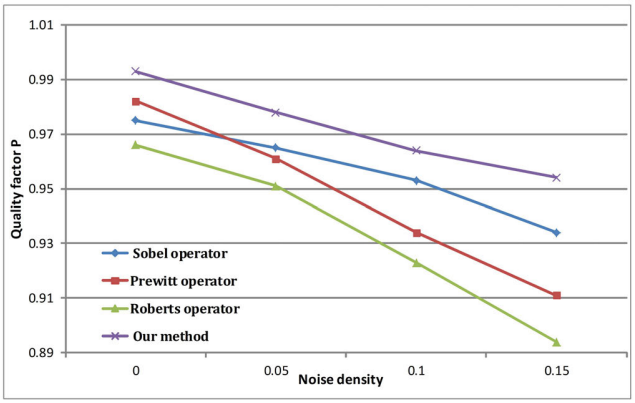

FIGURE 9. Comparison of road quality factor value and salt-and-pepper noise.

ratio and smoothness respectively. In practical application, the larger the overall evaluation index, we think the wavelet denoising effect is relatively better, see figures 5-6.

C. QUANTITATIVE ANALYSIS

In order to verify the generality of the algorithm and the reliability of the evaluation, a comparative experiment is carried out between the original gray-scale road remote sensing

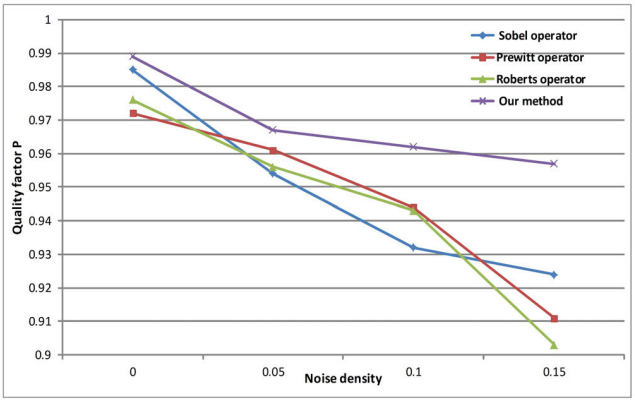

FIGURE 10. Comparison of highway quality factor value and salt-and-pepper noise.

image and the original gray-scale road remote sensing image in noisy and noisy environments. The quality factor P, which is comprehensively considered in the aspects of edge line loss and error detection and edge point positioning error, is used to evaluate the edge detection effect, namely as equ

$$P = \frac{1}{\max(I_l, I_a)} \sum_{i=1}^{I_l} \frac{1}{1 + \alpha d^2(i)}. \tag{43}$$

where I_l is the ideal number of edge points; I_a is the number of edge points actually detected; d is the distance between the ideal edge point and the actual edge point; α is a constant, usually 0.1. If the obtained P value is larger, the better the detected edge result is.

Figures 7-8 are Gaussian noise-quality factor graphs of the original gray road remote sensing image and the original gray road remote sensing image. Figures 9-10 are graphs of their salt and pepper noise-quality factor. It can be seen that the quality factor values of the edge detection evaluation results of the algorithm in this article are always higher than those of the other three algorithms under different intensity noises. Objectively, the edge detection effect of this algorithm is better, especially in noisy environment.

As can be seen from the above figures, the method proposed in this article has obvious advantages over other algorithms in quality factors.

VI. CONCLUSION

Under different noise levels, the wavelet is used for denoising and then combined with the morphological gradient operator. The noise of the original image is processed by wavelet, and the image with reduced noise is more effective for the later edge detection. In the experiment, the 3 × 3 median filtering Sobel operator, Roberts's operator, Prewitt operator and wavelet and morphological gradient operator method proposed in this article are used to detect the edge of Lena image. Although the Sobel operator has better edge detection capability, it has the worst anti-noise performance. The Roberts operator first 3 × 3 median filtering and then morphological

gradient operator, and the edge detection performance is better in low noise. The Prewitt operator performs better at edge detection at 20% noise level. The wavelet and morphological gradient operators proposed in this article, because in the quantum superposition state structural elements, the elements corresponding to the noise collapse to 0, do not participate in the morphological gradient operation, and the pulse noise intensity increases as compared with the reference image. The normalized mean square error increases slowly and shows good noise immunity; the edge detection result is consistent with the reference image when there is no noise.

REFERENCES

[1] M. A. Lefsky, W. B. Cohen, G. G. Parker, and D. J. Harding, "Lidar Remote Sensing for Ecosystem Studies: Lidar, an emerging remote sensing technology that directly measures the three-dimensional distribution of plant canopies, can accurately estimate vegetation structural attributes and should be of particular interest to forest, landscape, and global ecologists," *Psychol. Reports.*, vol. 46, no. 1, pp. 927–930, 2002.

[2] M. Janalipour and M. Taleai, "Building change detection after earthquake using multi-criteria decision analysis based on extracted information from high spatial resolution satellite images," *Int. J. Remote Sens.*, vol. 38, no. 1, pp. 82–99, Jan. 2017.

[3] W. Jiang, D. Carter, H. Fu, M. Jacobson, K. Zipp, J. Jin, and L. Yang, "The impact of the biomass crop assistance program on the United States forest products market: An application of the global forest products model," *Forests*, vol. 10, no. 3, pp. 1–12, Feb. 2019.

[4] J. Zhang, P. Zhou, and Q. Zhang, "Low-light image enhancement based on iterative multi-scale guided filter retinex," *J. Graph.*, vol. 39, no. 1, pp. 1–11, 2018.

[5] J. Zhu, J. Zhou, and C. Zhou, "A new combination filtering method to remove mixed noise of remote sensing images," *Geomatics Inf. Sci. Wuhan Univ.*, vol. 42, no. 3, pp. 348–354, 2017.

[6] D. Kincaid and W. Cheney, *Numerical Analysis: Mathematics of Scientific Computing*, 3rd ed. Beijing, China: China Machine Press, 2005, pp. 276–286.

[7] J. Zhang, "Image edge detection based on wavelet NSCT transform and mathematical morphology," Northeast Petroleum Univ., Heilongjiang, China, Tech. Rep., 2014, doi: CNKI:CDMD:2.1014.390455.

[8] J. Preciozzi, A. Almansa, P. Muse, S. Durand, A. Khazaal, and B. Rouge, "A sparsity-based variational approach for the restoration of SMOS images from L1A data," *IEEE Trans. Geosci. Remote Sens.*, vol. 55, no. 5, pp. 2811–2826, May 2017.

[9] H. Fan, Y. Chen, Y. Guo, H. Zhang, and G. Kuang, "Hyperspectral image restoration using low-rank tensor recovery," *IEEE J. Sel. Topics Appl. Earth Observ. Remote Sens.*, vol. 10, no. 10, pp. 4589–4604, Oct. 2017.

[10] X. Deng, Y. Du, and C. Y. Wang, "An adaptive threshold corner detection algorithm based on auto-correlation matrix of image pixel," *Trans. Chin. Soc. Agricult. Eng.*, vol. 33, no. 18, pp. 134–140, 2017.

[11] J. Bai, C.-C. Chang, T.-S. Nguyen, C. Zhu, and Y. Liu, "A high payload steganographic algorithm based on edge detection," *Displays*, vol. 46, pp. 42–51, Jan. 2017.

[12] F. O. Guillén-Reyes and F. J. Domínguez-Mota, "Boundary layer detection techniques applied to edge detection," *Int. J. Image Graph.*, vol. 19, no. 2, Apr. 2019, Art. no. 1950010.

[13] B. Yang, Y. Pi, X. Li, and M. Wang, "Relative geometric refinement of patch images without use of ground control points for the geostationary optical satellite GaoFen4," *IEEE Trans. Geosci. Remote Sens.*, vol. 56, no. 1, pp. 474–484, Jan. 2018.

[14] F. Shahzad, R. U. Haq, and Q. M. Al-Mdallal, "Water driven Cu nanoparticles between two concentric ducts with oscillatory pressure gradient," *J. Mol. Liquids*, vol. 224, pp. 322–332, Dec. 2016.

[15] Y. Himeur and A. Boukabou, "Robust image transmission over powerline channel with impulse noise," *Multimedia Tools Appl.*, vol. 76, no. 2, pp. 1–23, 2017.

[16] B. Brekhna, A. Mahmood, and Y. Zhou, "Robustness analysis of superpixel algorithms to image blur, additive Gaussian noise, and impulse noise," *J. Electron. Imag.*, vol. 26, no. 6, pp. 1–6, 2017.

[17] K. M. Malik, S. M. Anjum, H. Soltanian-Zadeh, H. Malik, and G. M. Malik, "A framework for intracranial saccular aneurysm detection and quantification using morphological analysis of cerebral angiograms," *IEEE Access*, vol. 6, pp. 7970–7986, Jan. 2018.

[18] Z. Huang, J. Zhang, X. Li, and H. Zhang, "Remote sensing image segmentation based on dynamic statistical region merging," *Optik*, vol. 125, no. 2, pp. 870–875, Jan. 2014.

[19] L. Zhang, C. He, J. Li, Y. Wang, and Z. Wang, "Comparison of IDW and physically based IDEW method in hydrological modelling for a large mountainous watershed, northwest China," *River Res. Appl.*, vol. 33, no. 6, pp. 912–924, Jul. 2017.

[20] J. O. Aguilar, A. C. Atoche, R. C. Alvarez, J. V. Castillo, I. Villalon-Turrubiates, and O. Perez-Martinez, "Enhancement and edge-preserving denoising: An OpenCL-based approach for remote sensing imagery," *IEEE J. Sel. Topics Appl. Earth Observ. Remote Sens.*, vol. 9, no. 12, pp. 5482–5492, Dec. 2016.

[21] M. Ciecholewski, "River channel segmentation in polarimetric SAR images: Watershed transform combined with average contrast maximisation," *Expert Syst. Appl.*, vol. 82, pp. 196–215, Oct. 2017.

[22] N. Donia, "Application of remotely sensed imagery to watershed analysis a case study of lake Karoun, Egypt," *Arabian J. Geosci.*, vol. 6, no. 9, pp. 3217–3228, Sep. 2013.

[23] Y. Xiang, F. Wang, L. Wan, and H. J. You, "SAR-PC: Edge detection in SAR images via an advanced phase congruency model," *Remote Sens.*, vol. 9, no. 3, pp. 209–218, 2017.

[24] J.-C. Ni, Q. Zhang, Q. Yang, Y. Luo, and L. Sun, "Directional feature: A novel feature for group target detection in high resolution SAR images," *Remote Sens. Lett.*, vol. 8, no. 8, pp. 713–722, Aug. 2017.

[25] A. Sedaghat and N. Mohammadi, "Uniform competency-based local feature extraction for remote sensing images," *ISPRS J. Photogramm. Remote Sens.*, vol. 135, pp. 142–157, Jan. 2018.

[26] E. Nadernejad, S. Sharifzadeh, and H. Hassanpour, "Edge detection techniques: Evaluations and comparisons," *Appl. Math. Sci.*, vol. 2, no. 31, pp. 1507–1520, 2008.

[27] W. K. Pratt, *Digital Image Processing: PIKS Inside*. Hoboken, NJ, USA: Wiley, 2001.

[28] J. M. Prewitt, "Object enhancement and extraction," *Picture Process. Psychopictorics*, vol. 10, no. 1, pp. 15–19, 1970.

[29] M. Manikandan, M. Paranthaman, and B. N. Aadithiya, "Detection of calcification form mammogram image using canny edge detector," *Indian J. Sci. Technol.*, vol. 11, no. 20, pp. 1–5, 2018.

[30] K. Ding, L. Xiao, and G. Weng, "Active contours driven by region-scalable fitting and optimized Laplacian of Gaussian energy for image segmentation," *Signal Process.*, vol. 134, no. 5, pp. 224–233, May 2017.

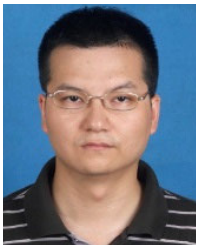

CHEN GUOBIN was born in Yancheng, Jiangsu, China, in 1982. He received the master's degree in computer software and theory from Chongqing Normal University. He is currently pursuing the Ph.D. degree with the Chongqing University of Posts and Telecommunications. Since 2010, he has been with the Rongzhi College, Chongqing Technology and Business University. He is currently an associate professor with the school. He has published more than 20 articles. His research interests include D2D networks, big data, machine learning, software architecture, web services, and intelligent information processing, and so on. He presided over the Chongqing Municipal Education Commission Science and Technology Project, Chongqing Science and Technology Innovation Project, and participated in the National Natural Science Foundation and the Chongqing Municipal Science and Technology Commission Project.

ZENGWU SUN was born in Tai'an, Shandong, China, in October 1986. He received the Ph.D. degree in engineering from the University of Chinese Academy of Sciences, Beijing, China. Since 2015, he has been a Teacher with the College of Medical Information Engineering, Shandong First Medical University and Shandong Academy of Medical Sciences, where he is currently a Lecturer. His research interests include information selecting and processing, pattern recognition, and image processing. He has published several research articles in scholarly journals in the above research areas and has participated in several conferences.

LI ZHANG was born in 1976. He received the master's degree in computer application from the Institute of Artificial Intelligence, Zhejiang University, and the Ph.D. degree in military logistics from the Department of Logistics Information Engineering, Logistic Engineering University. He is currently pursuing the Ph.D. degree. He is currently a Professor with the Rongzhi College, Chongqing Technology and Business University, a Visiting Scholar of Logistics and Supply Chain with the University of Missouri–St. Louis Business School, USA. He has published more than 40 academic articles. His main research interests include supply chain management, logistic system optimization, intelligent logistics, multi-agent systems, knowledge engineering, data mining, and so on. In recent years, he has undertaken or participated in 18 scientific research projects, such as the National Natural Science Foundation of China and the National Social Science Foundation of China.